Additive Manufacturing 25 (2019) 563–578

Contents lists available at ScienceDirect

Additive Manufacturing

journal homepage: www.elsevier.com/locate/addma

Full Length Article

Novel sprue designs in metal casting via 3D sand-printing

Santosh Reddy Sama[a], Tony Badamo[b], Paul Lynch[c], Guha Manogharan[a,*]

[a] Department of Mechanical and Nuclear Engineering, Pennsylvania State University, State College, PA, 16801, United States
[b] Hazleton Casting Company, Hazleton, PA, 18202, United States
[c] Department of Industrial Engineering, Penn State Behrend, Erie, PA, 16563, United States

ARTICLE INFO

Keywords:
3D sand-printing
Metal casting hydrodynamics
Gating system
Sprue
Flow simulation
Casting defects

ABSTRACT

The opportunity to improve the quality of metal castings by enabling fabrication of complex gating systems via 3D Sand-Printing (3DSP) has been recently established. Among the different components of a gating system (often called rigging), sprue design offers a major opportunity to exploit the unlimited geometric freedom offered by 3DSP process. In this study, conventional principles of casting hydrodynamics is advanced by validated novel numerical models for novel sprue designs to improve melt flow control. Computational flow simulations demonstrate that conical-helix sprue satisfy the critical velocity condition by reducing the ingate velocity below 0.5 m/s. Multiple approaches to integrate 3DSP into conventional manufacturing to fabricate complex gating systems through "Hybrid Molding" are presented. 3DSP molds featuring two optimized sprue profiles and a benchmark straight sprue are fabricated to pour 17-4 stainless steel. Computed tomography scans (CT) shows that parabolic sprue casting (PSC) and conical-helix sprue casting (CHSC) reduced overall casting defects by 56% and 99.5% respectively when compared to straight sprue casting (SSC). Scanning electron microscopy (SEM) analysis confirms the presence of globular oxide inclusions and that PSC and CHSC exhibits 21% and 35% reduced inclusion when compared to the SSC. Three point flexural testing reveals that CHSC and PSC exhibits an increase of 8.4% and 4.1% respectively in average ultimate flexural strength than SSC. The findings from this study demonstrate that numerically optimized gating systems that can only be fabricated via 3DSP have the potential to significantly improve both mechanical and metallurgical performance of sand castings.

1. Introduction

The market size of the metal casting industry was 20.23 billion USD in 2017 and is expected to grow annually at a rate of 8.87% to reach 39.94 billion USD by 2025 [1]. Engineered castings constitute about 90% of total manufactured goods and capital equipment [2]. In United States, over 2000 metal casting facilities employ more than 200,000 people across the country [2]. Despite having a casting market share of 80% [3], sand casting foundries across the globe suffer from long lead times, expensive tooling and limited flexibility. It is well known that the pattern making step in sand casting is the bottleneck and often, the most expensive component in low volume production runs. The need to remove the pattern from compacted sand mold to create casting cavity significantly restricts the geometries in traditional sand castings. The increased complexity of metal parts for industrial and mission critical applications demands new technologies. Recent advancements in 3D Sand-Printing (3DSP) which is a form of Additive Manufacturing (AM) bridges this technological gap through direct printing of sand molds in a layer-by-layer process [4,5].

3DSP is a binder-jetting AM process where foundry sand is spread in layers and binder (e.g. furan) isselectively deposited based on the computer aided design (CAD) file of the molds and cores. 3DSP offers a novel solution for directly fabricating molds and cores without any requirement of tooling [4]. The rapidly evolving AM technology has provided several opportunities to help the metal casting industry. Complex soft tools and hard tools such as jigs, fixtures and patterns can be fabricated using a range of AM processes and materials [6]. Patterns for sand casting can be directly printed plastic using material extrusion and vat photopolymerization systems [5] or wax for investment casting [7]. Fig. 1 illustrates the research framework for advancing metal casting applications by exploiting design freedom in 3DSP.

Mold filling is a critical phenomenon that directly impacts the quality of castings. The filling process is typically comprised of free surface flow of the metal front inside the mold cavity [8]. The exposure of liquid metals to air and moisture during free surface flows results in the oxidation of melt surface leading to the formation of surface oxide films [9]. Folding of free dry oxide surfaces result in detrimental bifilms or double oxide films [10,11] that act as cracks to initiate failures [12].

* Corresponding author.
E-mail address: gum53@psu.edu (G. Manogharan).

https://doi.org/10.1016/j.addma.2018.12.009
Received 4 November 2018; Received in revised form 10 December 2018; Accepted 11 December 2018
Available online 12 December 2018

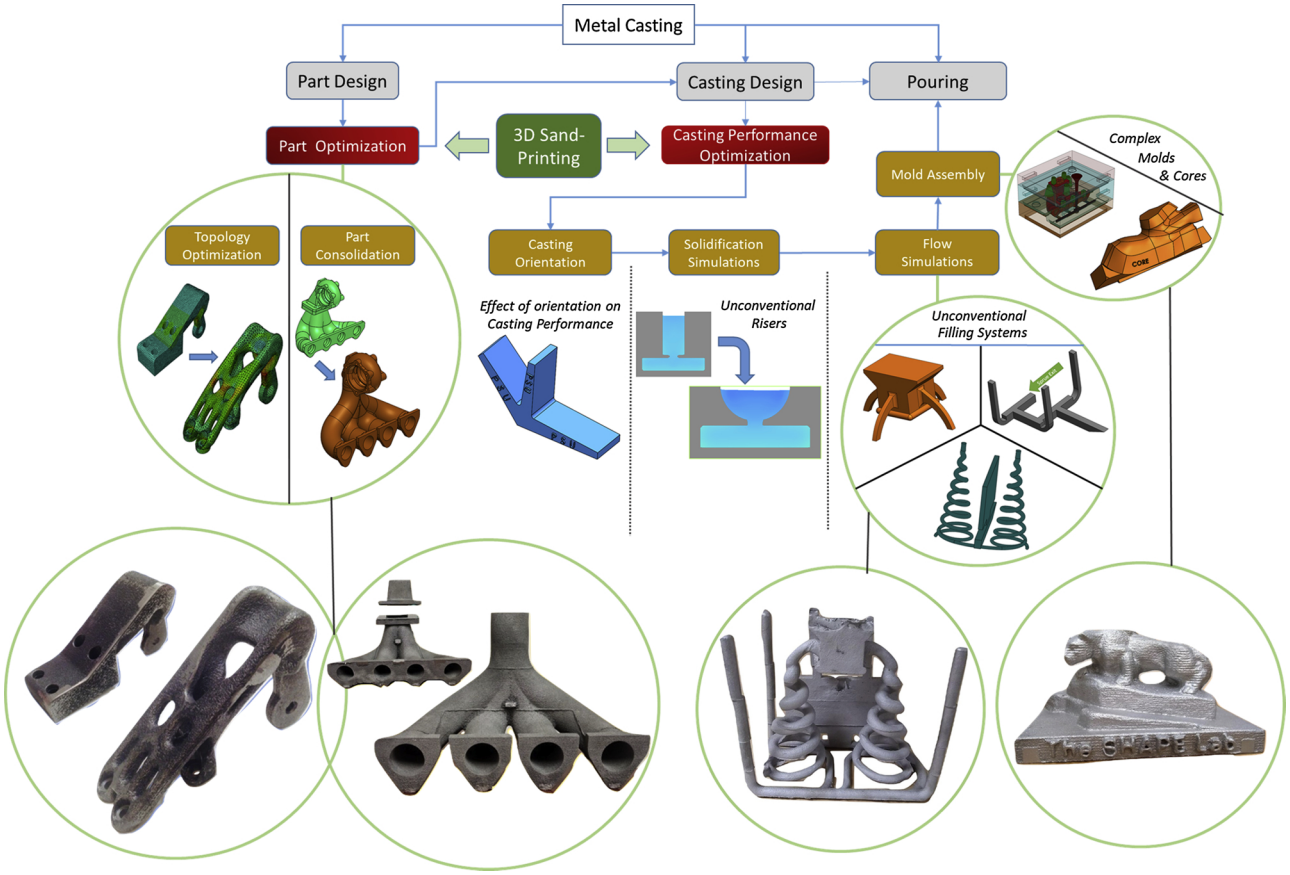

Fig. 1. Framework for 3D Sand-Printing Research Concepts.

The rate of bifilm formation increases with increase in turbulence as the oxide layers continuously stretch, rupture and regrow [13,14]. Entrained defects viz. surface oxides, oxide inclusions, sand inclusions, blowholes, bubbles, bifilms among others are significantly detrimental to the mechanical properties of castings [15–18]. Oxide films are found to adversely affect tensile strength [19–21], fatigue life [22], fracture strength [23], machinability [24,25] and also act as initiation sites for shrinkage pore formation [26] and hydrogen gas pore formation [27] in castings. Therefore, it is of most importance to reduce defects due to entrainment since they acause 80% of the total effective problems in castings [28]. Therefore, in order to make homogeneous castings with minimum scrap rate, it is critical to incorporate proper gating systems that facilitate effective control over mold filling by reducing velocity of liquid metal at ingate to less than 0.5 m/s [29,30] which will improve product quality and foundry productivity.

Since the sprue controls the fill rate of the casting, sprue is regarded as the “single most important part [31]” and “most critical component [32]” of the gating system”. During the filling process, liquid fall will act as plunging jet if the sprue is not filled completely [33] leading to gas entrainment [34,35]. Therefore, the liquid metal is usually choked at the bottom of the sprue and the filling rate of the mold cavity is controlled by changing the cross sectional area at the sprue exit [36]. However, Campbell notes that an ideal design should use the entire length of the sprue to control the flow rate [8]. Campbell further mentions “Although methoding engineers have been carrying out such calculations correctly for many years, somehow only the sprue exit has been considered to act as the choke [8]”. The authors in this research propose that if carefully designed, it is feasible to control the rate of the metal flow all through the length of the sprue via 3DSP. Therefore, in order to reduce casting defects, gating systems must be redesigned for 3DSP which does not suffer from severe hard tooling requirements of conventional mold-making process.

In this research, numerical models for two complex sprue profiles are developed and their effects on casting performance are experimentally validated. Novel methods to fabricate complex conical-helix sprue channels (CHSC) via “hybrid molding” approaches are presented. Section 2 presents a brief literature review of reported studies on optimizing gating systems. Section 3 details the numerical models and optimization algorithm for the novel complex sprue concepts. Section 4 details the design of experiments including steps to fabricate 3DSP molds and castings. Section 5 presents both computational and experimental results and Section 6 analyses the relevance of the results. Finally, Section 7 summarizes this study along with brief discussion on future directions of this research.

2. Literature review and research gap

In the past century, researchers have experimented with various parameters for construction of straight sprue based on the basic principles of fluid dynamics. Most of the current design knowledge on gating systems are derived from trial and error approaches [36,37], water modelling [35,38,39] and more recently, using computational simulation tools [40–42]. Since the kinematic viscosity of most liquid metals is similar to water [35,37,38,43], numerous researchers have experimented with water models using transparent molds usually made of Perspex [38] or acrylic [44] to visualize fluid flow in molds. More accurate visualizations to overcome the limitations of water analogs are feasible through real-time X-ray imaging during mold filling [45,46]. However, this system is very expensive and only offers qualitative information.

Interfacial fluid modelling by tracking free surfaces can be employed using Eulerian techniques through marker method and volume-of-fluid (VOF) methods [47] or by using Lagrangian methods such as smoothed-particle hydrodynamics [48]. Most commercial simulation

Table 1
Nomenclature for sprue design.

α	Angular frequency of conical-helix
r	Parameter related to radius of the cone in conical-helix
$a,\ b$	Parameters that defines parabolic profile
h_{sprue}	Total height of the sprue (m)
h_{basin}	Depth of the pouring basin (m)
$h_{f_{dt}}$	Total head loss when liquid traverses through a $3d$-profile of length dt (m)
g	Acceleration due to gravity (m/s^2)
t	Parameter to define depth from top of sprue
$s(t)$	Length of the profile from top of sprue (m)
$d(t)$	Diameter of the cross section of the sprue channel at depth t (m)
v_t	Velocity at a depth t from top of the sprue (m/s)
dt	Incremental depth (m)
f	Friction factor
K_b	Bend loss coefficient
Re	Reynolds Number

packages (Ex: MAGMAsoft, Flow3D) utilize the VOF method to model castings. Gating systems are typically analyzed using computational modelling, statistical or mathematical optimization algorithms or a combination of these techniques. Trident gates, spin traps and bubble traps are found to be effective in reducing melt turbulence through computational simulations for cast steel [49]. Runner depth and runner tail slope are optimized for aluminum by coupling the Sequential Quadratic Programming (SQP) direct gradient optimization algorithm in flow simulations [50]. Ingate height, ingate width, runner height and runner width are optimized to minimize shrinkage porosity, filling velocity and improve product yield in cast magnesium cylindrical housings using Taguchi statistical tools [42]. Another study focused on optimizing the geometrical descriptors viz. radii of the ingates and runner to minimize liquid metal velocity using Pareto front based multi-objective evolutionary algorithm [51].

Alternative to optimizing parameters of conventional gating systems, few studies in the literature reported on modifiying conventional sprue designs to minimize oxide film formation. An off-set sprue that feature a double-perpendicular turn at the intersection of the sprue/runner junction was shown to be effective in reducing melt turbulence while decreasing the in-gate velocity below 0.5 m/s [33]. However, fluid flow through double-perpendicular bend is more prone to forming low pressure vortexes at the junction which will react with the melt flow resulting in the formation of oxides [33,52]. Another study proved this by demonstrating a smooth L-shaped curvature at the sprue/runner junction to lower turbulence without entrapping any detrimental oxide films [53]. A vortex well at the intersection of the sprue and runner which was manufactured using a pattern via multi jet modelling AM technology provided early evidence of enhanced mechanical and microstructure properties of cast parts [54].

Fig. 1 shows that by leveraging shape complexity of the 3DSP process, part optimization and/or casting performance optimization can be performed. In the part optimization module, the feasibility of manufacturing complex topology optimized structures is demonstrated [5]. Additionally, functional components can be consolidated to minimize weight such as the elimination of flanges by consolidating geometry of an exhaust manifold and the base of a turbine housing as shown in Fig. 1. The opportunity via 3DSP to optimize casting performance by using non-conventional gating and feeding systems has recently been established [52]. Casting orientation can be optimized independent of tooling requirements for optimal casting performance and numerically optimal hemi-spherical risers is feasible via 3DSP. Pouring basins with lateral outlets, multiple sprues, complex runners and ingates as shown in Fig. 1 could facilitate better turbulence control. The ability to print complex molds and cores can be exploited to increase casting performance, e.g. shell-truss molds to tailor cooling rate per specific casting requirements [55].

Water-analog experiments and limited validation through current X-ray imaging demands prototype molds that are not only expensive but also have limited geometrical flexibility. It makes such techniques extremely challenging and time consuming for analyzing optimal gating solutions. This research aims to explore the 'rapid production' capability of 3DSP technique to discover optimal gating systems with novel design concept that are extremely difficult to fabricate via any traditional manufacturing process. The application of optimization algorithms based on principles of casting hydrodynamics to satisfy ideal mold filling conditions are examined and validated using computational simulations, casting defects characterization and mechanical testing. This comprehensive research demonstrates the potential of design freedom via 3DSP to incorporate numerically optimized gating design for any given casting to produce defect-free cast parts.

3. Sprue modelling

Based on well-established studies in casting hydrodynamics, three prominent design conditions should be satisfied in an optimal sprue to reduce entrainment:

1 Velocity at the ingate should be less than or equal to critical velocity (0.5 m/s) implying that the velocity at the bottom of the sprue is constrained [8,16,29,30]
2 Minimize the overall length of the sprue to minimize thermal loss [56] and provide adequate time for generated gas bubbles to escape the mold [35]
3 Abrupt changes either in the sprue profile or at the intersection of sprue with the runner bar should be avoided [8,16]

3.1. Velocity after a generic fluid fall

Fluid flow in a sprue is approximated as a Newtonian fluid flow with frictional effects in a circular channel with surface roughness. The objective for developing an optimal numerical model is to strategically harness the wall-melt flow frictional forces to decrease the velocity of the melt at the ingate below critical velocity. Table 1 provides the nomenclature of variables for sprue design. Applying Bernoulli's principle in a generic fluid fall of dt at a depth t as shown in Fig. 2, provides:

$$\frac{v_t^2}{2g} + dt = \frac{v_{t+dt}^2}{2g} + h_{f_{dt}} \tag{1}$$

$$h_{f_{dt}} = \frac{v_t^2}{2g}\left(\frac{f \times s(t)}{d(t)} + K_b\right) \tag{2}$$

The head loss due to friction ($h_{f_{dt}}$) is determined using Eq. (2) which is adopted from [36]. However, authors are not aware of analytical correlations that can provide bend head loss coefficient K_b for a generic three-dimensional curvature and hence K_b is not considered in this study. Substituting $K_b = 0$ in Eq. (2) gives the Darcy-Weisbach equation

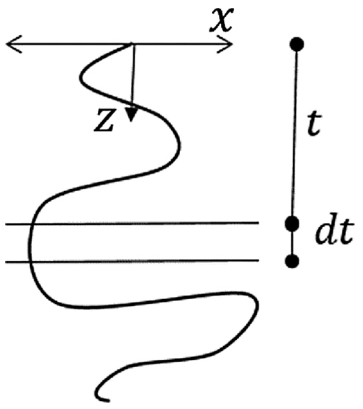

Fig. 2. A generic metal fall of dt at depth.t.

since the metal flow in a gating system lies in the turbulent regime (Re > > 2000). The analytical correlation for Moody's friction factor f [57] is calculated using Haaland equation [58] given in Eq. (3). For any given sprue profile, assuming a constant metal input velocity of $v_{t=0} = \sqrt{2gh_{basin}}$ at the top of the sprue, the velocity of the metal at any given depth v_t is determined using Eq 1. In order to obtain velocity at the bottom of the sprue $v_{t=h_{sprue}}$, Eq. 1 is applied incrementally multiple times (i.e. h_{sprue}/dt).

$$\frac{1}{\sqrt{f}} = -1.8log\left[\left(\frac{\varepsilon/d(t)}{3.7}\right)^{1.11} + \frac{6.9}{Re}\right] \tag{3}$$

3.2. Mathematical profiles

Conical-helix and parabolic sprue profiles [52] are considered in this study and preliminary simulations showed the former profile is the most optimal sprue configuration. The parameters that define the two complex profiles and the formulation of length of the sprue are discussed in this section.

3.2.1. Conical helix sprue casting (CHSC)

The parametric equations that define a conical-helix profile shown in Fig. 3 are given in Eq. (4):

$$\begin{aligned} x &= tr\cos(\alpha t) \\ y &= tr\sin(\alpha t) \\ z &= h_{sprue} - t \end{aligned} \tag{4}$$

Here r is proportional to the radius of the overlaying cone with inverse of height of sprue as the constant of proportionality. α is equal to the angular frequency of the helix. Length of the curve from the top of the sprue at depth t in conical helix profile is given in Eq. (5):

$$s(t) = \frac{1}{2}t\left[\sqrt{1 + r^2(1 + \alpha^2 r^2)}\right] + \frac{1 + r^2}{2\alpha r}\sinh^{-1}\frac{\alpha r t}{\sqrt{1 + r^2}} \tag{5}$$

The upper bound for the angular frequency is defined to by constraining metal fall to be lower than critical fall height h_{cr} as shown in Eq. (6). Critical height is equal to the height of sessile drop of a metal and is $10mm - 15mm$ for most metals [8,16].

$$\alpha < \alpha_{cr} = \frac{2\pi}{h_{cr}} \tag{6}$$

3.2.2. Parabolic sprue casting (PSC)

The origin of the parabolic profile is fixed at the bottom end of the parabolic sprue as shown in Fig. 4. Parametric equations for this parabolic configuration are given in Eq. (7) as:

$$y = a(x - b)^2 - ab^2 \tag{7}$$

The length of the curve from the top of the sprue is given in Eq. (8) as:

$$s(t) = L(x(t)) - L(x(0)) \tag{8}$$

$L(y)$ is the length of the curve from the bottom of the sprue and $x(t)$ is the x coordinate of the intersection of the profile at depth t from the top of the sprue as defined in Eqs. (9) and (10) respectively.

$$L(y) = \frac{(b - y)\sqrt{1 + 4a^2(b - y)^2}}{2} - \frac{\sinh^{-1}2a(b - y)}{4a} \tag{9}$$

$$x(t) = b - \sqrt{\frac{h_{sprue} - t}{a} + b^2} \tag{10}$$

3.3. Optimization algorithm

A constrained optimization algorithm is presented to minimize the length of the profile to reduce thermal loss and concurrently ensure the target velocity condition is achieved. The optimization problem can be summarized as:

Objective: Minimize length of the curve $s(t)$
Constraint: $v_{t=h_{sprue}} \leq v_{target}$
Variables: α, r for conical-helix
a, b for parabolic

The Sequential Quadratic Programming (SQP) constrained optimization algorithm is implemented using the MATLAB inbuilt *fmincon* function. The rationale behind using SQP technique is its demonstrated utility for gating system optimization and application of the VOF method for CFD analysis which were in agreement to real-time experiments [50,59]. The flow chart shown in Fig. 5 summarizes the optimization routine. v_{bottom} is calculated based on procedure in Section 3.1 and the length of the profile $s(t)$ is determined based on procedure in Section 3.2.

3.4. Convergence study

This section discusses if the optimization algorithm converges to a

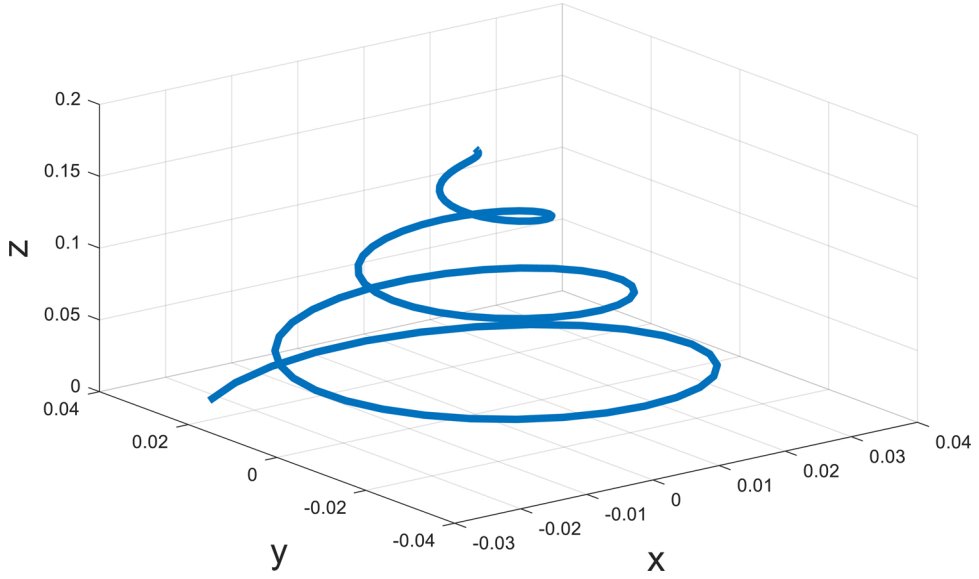

Fig. 3. A generic conical-helix sprue profile (CHSC).

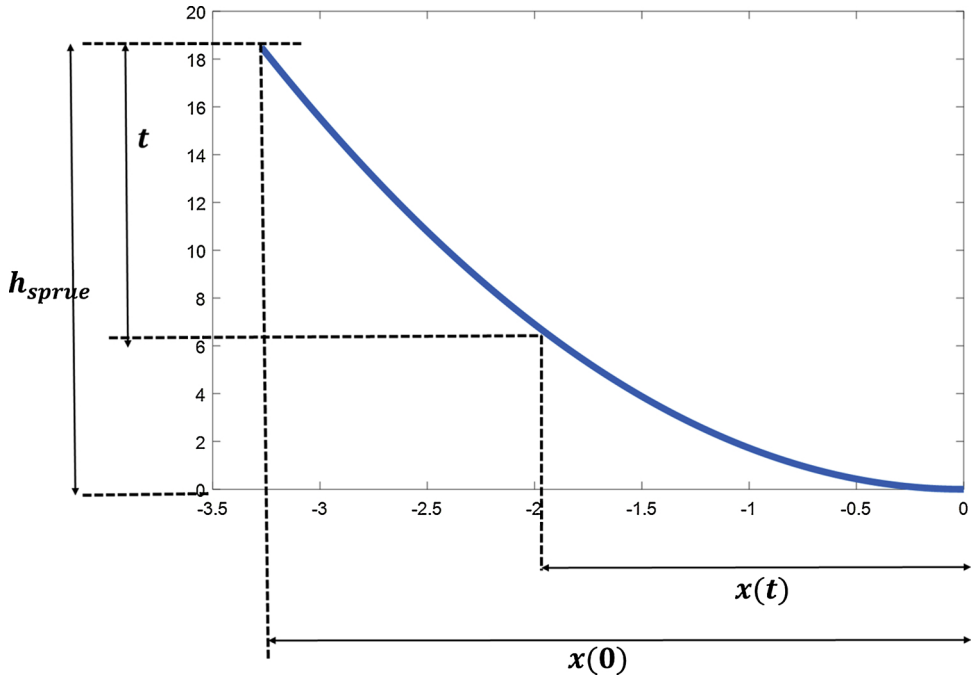

Fig. 4. A parabolic sprue profile with origin at the bottom end of the sprue casting (PSC). Parameters a, b are optimized to find.$x(0)$.

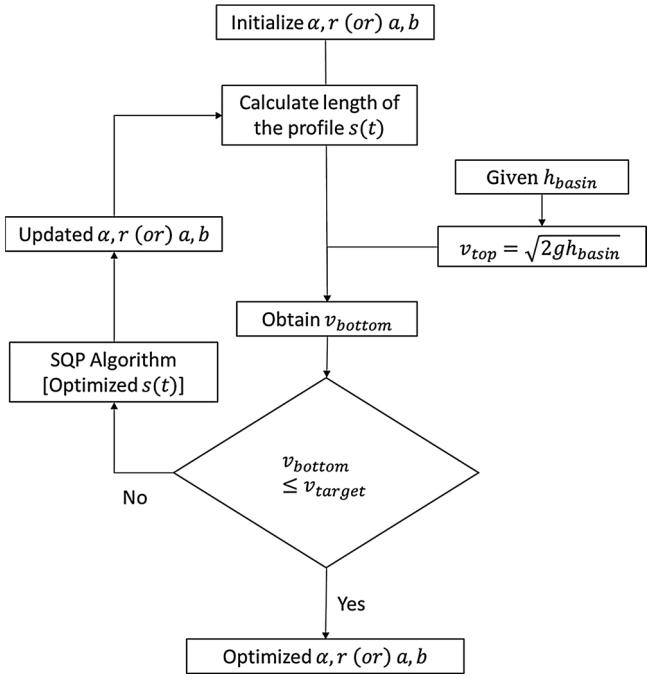

Fig. 5. Flow chart of the 3DSP sprue design optimization algorithm.

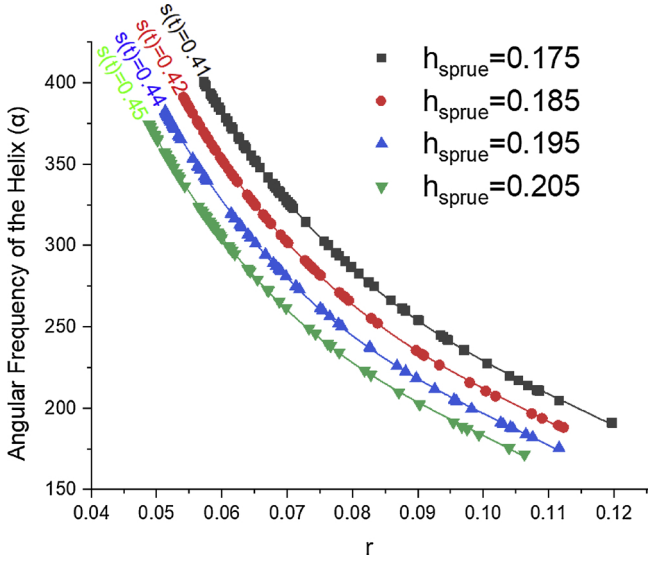

Fig. 6. Convergence analysis of optimization variables for CHSC (Units are in mm).

unique solution for a given pouring condition. A unique solution exists with unique parameters for the parabolic profile irrespective of the initial conditions. However, in the case of conical-helix profile, a unique optimal length of the curve exists but infinite possibilities for the parameters α, r are available to achieve the derived optimum. An illustration of the various combinations of α, r for optimal length for different sprue heights in conical-helix is shown in Fig. 6. An increase in length of the sprue $s(t)$ is observed as the height of the sprue is increased. A unique solution would be feasible if the bend loss friction factor K_b was considered in the formulation of head loss, which will be included in future work. In this study, the profile that has maximum bends i.e., high α value or low r value is considered as an optimal solution because of its potential to increase frictional losses. It should be noted that the 3D channel which follows a conical-helix profile is designed by extruding tapered circular cross section on the optimized conical-helix space curve. Therefore, design for manufacturing demands that global optimum parameters are selected based on not just maximizing α but also considering the feasibility of fabricating a circular cross section through the conical-helix space curve.

4. Experimental procedure

4.1. Mold design

In this research, 17-4 stainless steel alloy (martensitic stainless steel containing 3 wt.% Cu) was poured into 3DSP molds of straight sprued casting (SSC), parabolic sprued casting (PSC) and conical-helix sprued

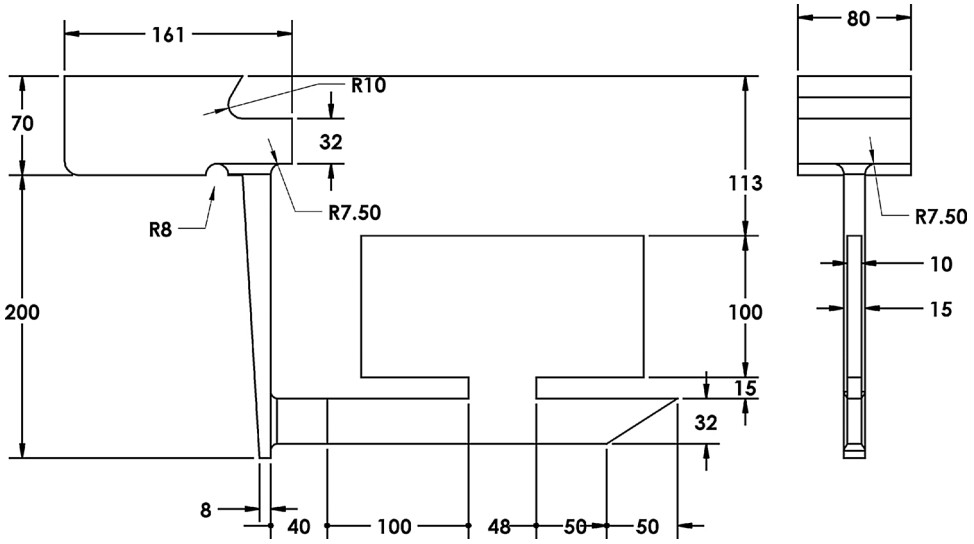

Fig. 7. Dimensions of the pouring basin, runner, ingate and cast part are constant for all sprue designs.

casting (CHSC). 17-4 stainless steel is a martensitic stainless steel widely used for corrosion-critical components. The sub-sections below describe the optimal sprue design parameters and mold dimensions.

4.1.1. Design of sprue

The benchmark cast part and gating system geometry were adopted from Yang et al [33]. The height of the sprue was always maintained at 185 mm [33]. The advantage of the undercut at the base of pouring basin include minimizing the occurrence of splashing and the sprue cover prevents metal from directly falling into the sprue [16]. Unlike conventional mold making [16], incorporation of these additional design features is relatively easier and cheaper with 3DSP molds. The pouring basin is altered from [33] and is redesigned as shown in Fig. 7. While the sprue well is provided in conventional straight sprue [33], it is not provided in PSC and CHSC as recommended by Campbell [16].

The average roughness of the surface of mold wall ε required in the formulation of friction factor was approximated as 5μm using a C-9 cast microfinish comparator as per ANSI/ASME B46.1 [60] after mold wash. Mold wash is a commonly employed step in foundries prior to pour where an alcohol-based liquid is applied on mold surfaces that will interact with liquid metal and is ignited to improve mold surface quality. In this study, mold wash from ASK Chemicals supplied by Lancaster Foundry Supply Company is applied prior to pour. The density of 17-4 stainless steel liquid metal is 7030 kg/m^3 with a kinematic viscosity of 90 $\mu m^2/s$ [61]. The optimization algorithm detailed in Section 3 yielded $s(t)$ of 372 mm and 423 mm for PSC and CHSC configurations respectively when compared to 185 mm sprue length in SSC [33]. The optimum length in the CHSC could have been the least if K_b would have been considered in head loss formulation. Additional details for the different sprue configurations are listed in Table 2.

In order to design the subsequent components of the gating system i.e., runner and ingate geometries need to be analysed. A gating ratio of 1.5:4:6 was considered with a friction loss factor of 10% in the gating design wizard in SolidCAST [62] and the results are also included in Table 2. In order to isolate the effects of the proposed sprue designs, design parameters for pouring basin, runner, vent and cast part geometries were maintained uniform across the three configurations and their dimensions are shown in Fig. 7.

4.1.2. Mold fabrication and casting process

The molds were fabricated using a Viridis3D RAM printer with a layer thickness of 0.4 mm. ViriCast powder and CSTRed Binder (both produced by Viridis3D) were used in the printing process. Using sieve analysis, the AFS grain fineness number for the ViriCast powder was found to be 216 [63]. Mold wash was applied to all the internal surfaces of the mold as it was proven effective in changing the metal flow from chaotic to smooth [45]. After printing, loose sand was drained from internal cavities in the mold. Conical-helix channels were narrow and appropriate design considerations was undertaken to provide access for draining loose sand. There are multiple ways to incorporated drain access to remove loose sand from conical-helix sprues as illustrated in Fig. 8.

Table 2
Optimal Parameters for the three different gating system in this study.

Sprue	Parameter	Straight	Parabolic	Conical Helix
Top Cross Section	Area (mm^2)	300	310	310
	Length/Width or Diameter (mm)	20/15	19.8	19.8
Bottom Cross Section	Area (mm^2)	120	79	78.5
	Length/Width or Diameter (mm)	15/8	10	10
Profile Characteristics	Length (mm)	185	372	423
	r (mm), α	–	–	136, 156
	x_h (mm)	–	312	–

The categories ① and ② in Fig. 8 fall under the concept of “Hybrid Molding”, a term coined by authors to represent manufacturing techniques in which 3D sand-printed products are integrated into conventional molds to produce castings. Hybrid molding offers a platform to integrate the design complexity and rapid production of 3DSP with tooling available for conventional mold making (e.g. existing patterns and core boxes). In order to illustrate this approach, a conventional wooden pattern was fabricated along with a standalone 3DSP sprue which was later assembled with the pattern. In category ①, trapped sand was removed by designing the CHSC as a three piece system in which a core slices the conical-helix. In category ②, trapped sand was removed by providing multiple horizontal parting lines across sprue length. The categories ③ and ④ uses only 3DSP molds without using any pattern or core in two different parting line orientation. Material characterization experiments were performed only on castings made from category ③. The 17-4 stainless steel alloy was poured at 2950 °F and the pour time was tracked using stopwatch: 3.1s-PSC, 4s-SSC and 5.7s – CHSC. Fig. 9 shows examples of cast parts in the three different sprue configurations after mold shake out and sand blasting. Post-casting heat treatment processing were not employed in this study to isolate the effects of the novel sprue designs.

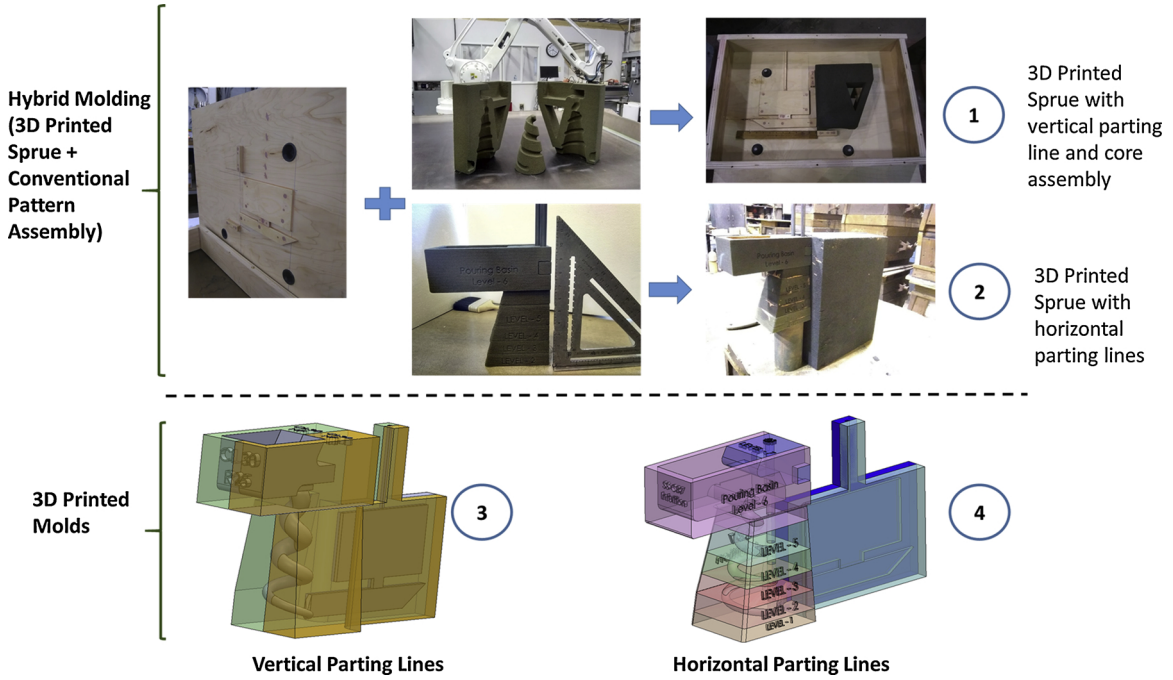

Fig. 8. Multiple techniques to fabricate CHSC (1) Hybrid molding with vertical split sprue and core assembly, and (2) Hybrid molding with horizontal parting lines; and 3D Printed molds with (3) vertical and (4) horizontal parting lines.

4.2. Flow modelling and characterization

Computational fluid flow modelling was performed in FLOW-3D CAST V4.2 (Flow Science) software with identical inlet, fluid and boundary conditions. The software applies Navier-Stokes methodology using VOF method and is consistent with actual flow patterns as revealed by radiography [19]. An inlet metal flow rate of 225 cm^3/s into the pouring basin was maintained constant in all three sprue designs. Probes were placed 5mm above the ingate along the mid-plane of the casting to calculate air entrapment (Section 5.1).

It is common to use destructive and non-destructive testing as a quality control tool to inspect internal flaws in castings. A GE v|tome|x Computed Tomography Scanning (CT) system with a 270 kV 300 μ A X-ray beam with a resolution of 112 μm per voxel was used to inspect casting defects. After segmentation, quantitative image analysis was conducted by cropping an identical sub-volume of $1651 \times 751 \times 53$ voxel space from all CT scans to eliminate surface scanning artifacts. The sub-volumes were converted to 16 bit images and gray scale value lower than 30,000 is applied as the threshold for casting defects. Authors believe that this is the first reported study which employs CT to quantify casting defects in evaluating gating systems.

In order to study the effects of gating system design on microstructure, one sample from each of the machined plates were cut using the water-jet process from identical locations in the castings. The samples were polished in an *Allied Multiprep System* to a $1\mu m$ finish in using a diamond-lapping film and *Greenlube* lubricant. Ten SEM observations per sample spanning across the sample surface were recorded using a *Thermo Fisher (FEI) Q250 Environmental* scanning electron microscope (SEM) which is also equipped with EDS capabilities. EDS was performed on the same polished surface to quantify the elemental composition of casting defects and base alloy.

Flexural testing using ASTM E290 standard [64] protocol was conducted to understand the effect of the filling system on mechanical strength. Four samples of $60 \times 12 \times 4.25\, mm^3$ were CNC machined from each of the three castings and were tested under a three point bending load in an *MTS Qtest Elite 100* machine. “Edge effects” that cause increased strength in samples from edges when compared to center are beyond the scope of this study and their effect is not considered [54]. Fig. 10 shows the locations for both flexural specimens and SEM/EDS microstructure specimen in the casting.

5. Results and discussions

5.1. Computational simulations

Mold filling simulations show that SSC is prone to severe undesired melt turbulence as melt flow velocity violate the critical velocity condition as shown in Fig. 11. It can be observed from Figs. 12 and 13 that PSC and CHSC facilitates relatively smoother metal flow at the bottom of the sprue and entirely adheres to the critical velocity condition at the ingate. In PSC and CHSC design concepts, the metal front is parallel to the runner which indicates laminar metal flow throughout the filling process. Conversely, the metal front in SSC is observed to fountain and fold over similar to prior studies [65,50,66] where extensive oxide films were reported.

Fig. 14 compares the air entrapped (% volume) in the melt collected by a virtual probe located 5 mm above the ingate at an identical location in all three sprue design flow simulations. It provides evidence that

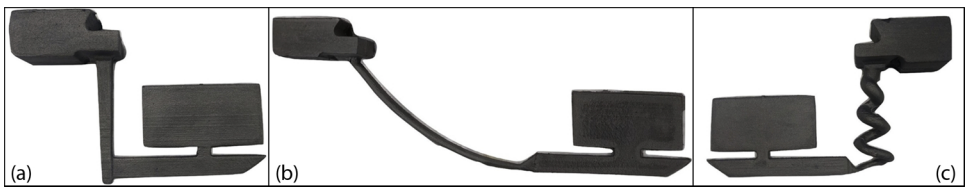

Fig. 9. 17-4 stainless steel alloy castings featuring (a) straight sprue (b) parabolic sprue casting (PSC)(c) conical-helix sprue casting (CHSC).

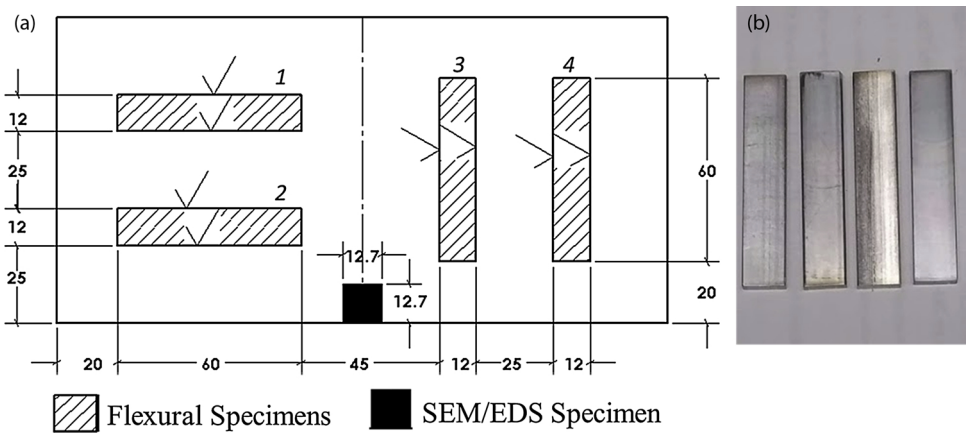

Fig. 10. (a) Location of four flexural specimens (60 × 12 × 4.25) and a SEM/EDSM microstructure specimen machined from each casting (in mm) (b) Machined flexural specimens from CHSC.

numerically optimized sprue geometries drastically reduces air entrapped by limiting turbulent flow. The characteristic peaks in the air entrapment profiles are due to the recirculation of fluid within the mold and their intensity increases with increase in turbulence.

5.2. CT scan

As mentioned in Section 4.3, scanning artifacts (such as edge blur image degradation) are addressed by cropping the edges of the CT images. The cropped volume consists of $1651 \times 751 \times 53$ matrix of voxels with a resolution of $112\mu m$ per voxel. Fig. 15 summarizes the results from CT scans and shows that PSC and CHSC reduces overall casting defects by 56% and 99.5% respectively when compared SSC. It is evident that CHSC demonstrates the ability to produce cleaner/denser castings that exhibit superior part performance characteristics (Section 5.4).

5.3. Microstructure and inclusion characterization

The microstructure of polished specimens was identical in all three sprue designs because the rate of solidification is not impacted by sprue design. Fig. 16 shows representative microstructures of SSC, PSC and CHSC. The dark circular regions that are dispersed in the microstructure in Fig. 16 are inclusions that are of interest in this study. EDS analysis of these inclusions revealed oxides with high silicon and aluminum content. Significant amounts of sulphur and manganese were also found. As shown in Fig. 17, the inclusions have similar elemental compositions in all three conditions. In summary, EDS analysis reveals that the casting defects are predominantly oxide inclusions and are found to be reoxidation macro-inclusions [67] (see Section 6.1) that are formed due to melt turbulence during the filling process.

Ten SEM images per sample were used to statistically evaluate the distribution of inclusions on the microstructure. These images were evaluated using an image analysis software (ImageJ [68]) and Fig. 16(d) summarizes the findings from inclusion distribution analysis. It was observed that PSC and CHSC exhibits a 21% and 35% reduction inclusion area when compared to SSC. A one-way Analysis of Variance (ANOVA) statistical test resulted in a p-value of 0.044 indicating that statistical significance of sprue design concepts on inclusion distribution ($\alpha = 0.05$). Tukey-Fisher statistical tests also established that the means of CHSC and SSC are significantly different.

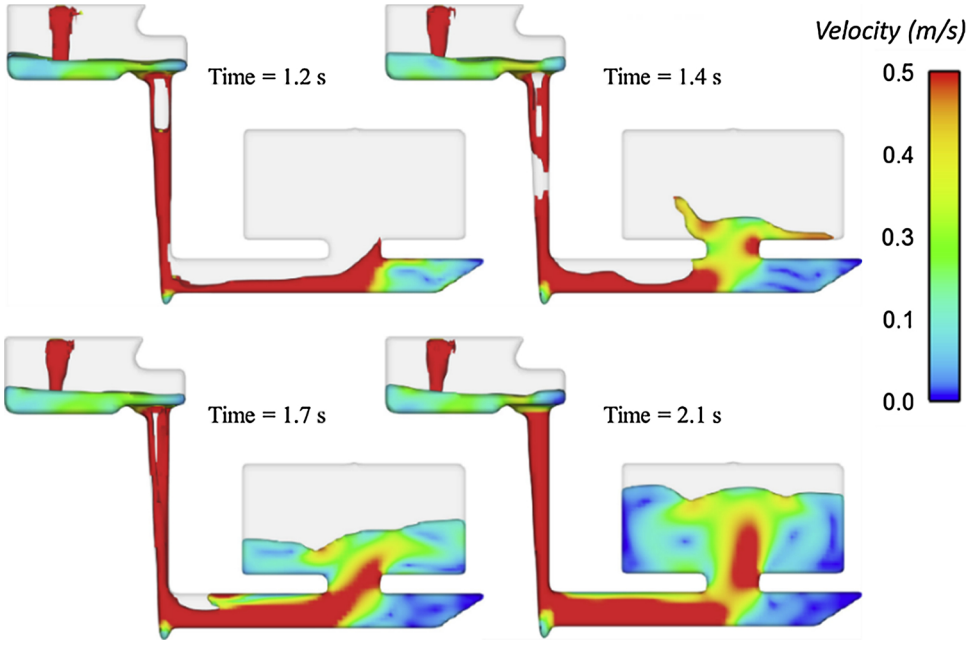

Fig. 11. Prediction of filling for a straight sprued castings at varying time steps.

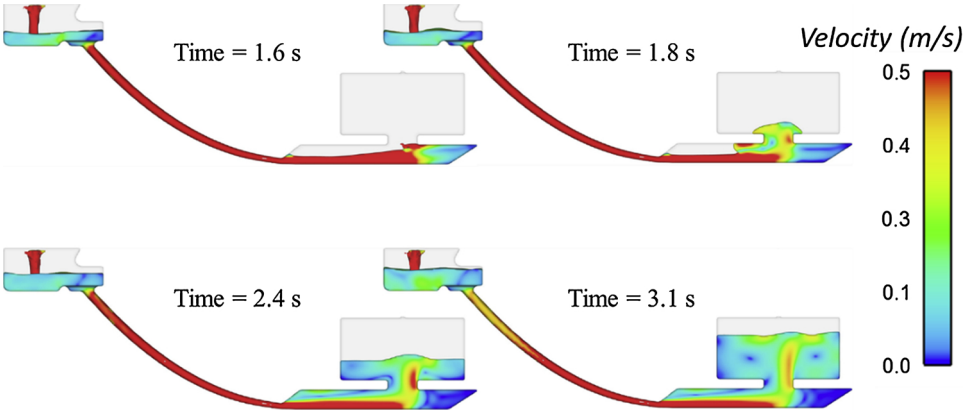

Fig. 12. Prediction of filling for a parabolic sprued casting at varying time steps.

5.4. Flexural strength

Ultimate flexural strength for the three castings is summarized in Fig. 18 and the results indicate that CHSC shows 8.4% enhanced mechanical strength when compared to SSC. As the limited sample size (n = 4) cannot be assumed to be normally distributed, non-parametric Friedman ANOVA test is conducted to test statistical significance between SSC and CHSC. The two tests reveal a *p-value* of 0.045. The conclusion from the Friedman ANOVA test was that a statistically significant difference occurred for ultimate flexural strength between SSC and CHSC. Statistically significance is not observed between SSC and PSC.

6. Discussions

6.1. Relevance of modelling and characterization to experimental observations

Optimization of SSC sprue design based on Flow3D simulations was in close agreement to real-time X-ray radiographic experiments [33]. The filling simulation of SSC in the present study shows that fountaining is directed towards the sprue when metal enters from ingate into the cast part as shown in Fig. 19(a). However, this is contrary to observations in Aluminum literature [65,33] and gray cast iron experimental observations [45] where the fountain almost always fountains away from the sprue as summarized in Fig. 19. This difference is attributed to the dynamic viscosity of liquid steel which is twice that of liquid aluminum resulting in molten steel in low-viscous laminar flow rather as opposed to turbulent flow as defined by Sirrel et al. [65]. Fountaining towards the sprue occurs when the overlying laminar reflected wave that has originated from the runner extension does not mix with the underlying turbulent flow [65].Since the length of the sprue (185 mm) used in this study is far less than the benchmark studies in Aluminum alloys (410 mm) [65], liquid metal would not experience as high of a degree of turbulence in the runner and gate in this study.

Reoxidation inclusions or “young oxide films” form when deoxidized steel comes into contact with oxygen/air during mold pouring and filling. It is estimated to cause 83% and 48% of macro-inclusions for low-alloy and high-alloy steel castings respectively [69] and this phenomenon was extensively investigated in the literature [70]. The “young” oxide films occurs as indigenous non-metallic inclusions that are generated during filling in the form of ‘tangled or network’, ‘layer oxide or globular oxide’ or ‘cloud or strip clustering particles’ [71]. The results from SEM in this study show that they take the form of globular oxides in 17-4 stainless steel alloy. This result is substantiated through EDS analysis which confirms the presence of oxides of silicon, aluminum and manganese similar to Steel Foundry Society of America (SFSA) research [72,73]. Aluminum oxides and silicates that are found

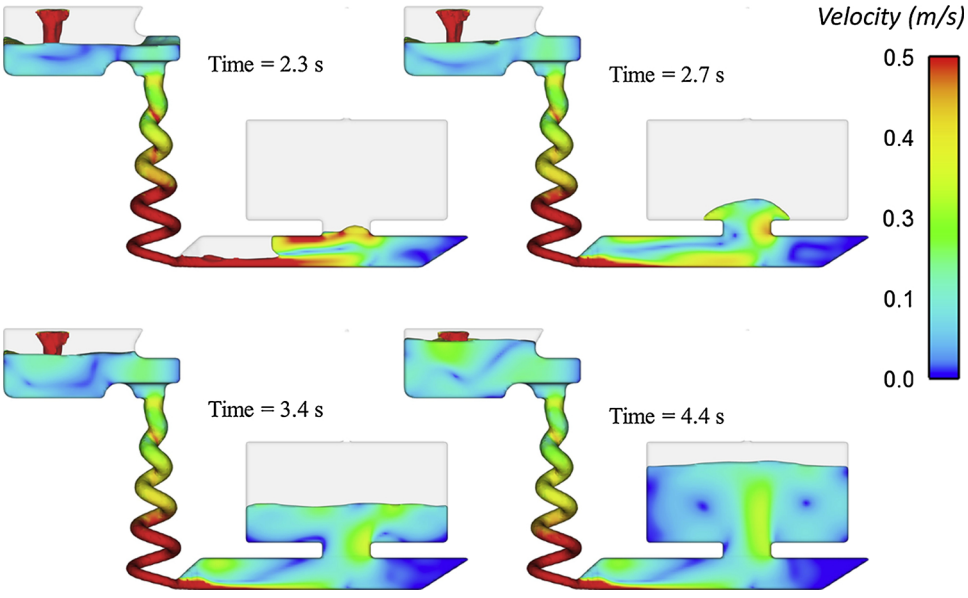

Fig. 13. Prediction of filling for a conical-helix sprued casting at varying time steps.

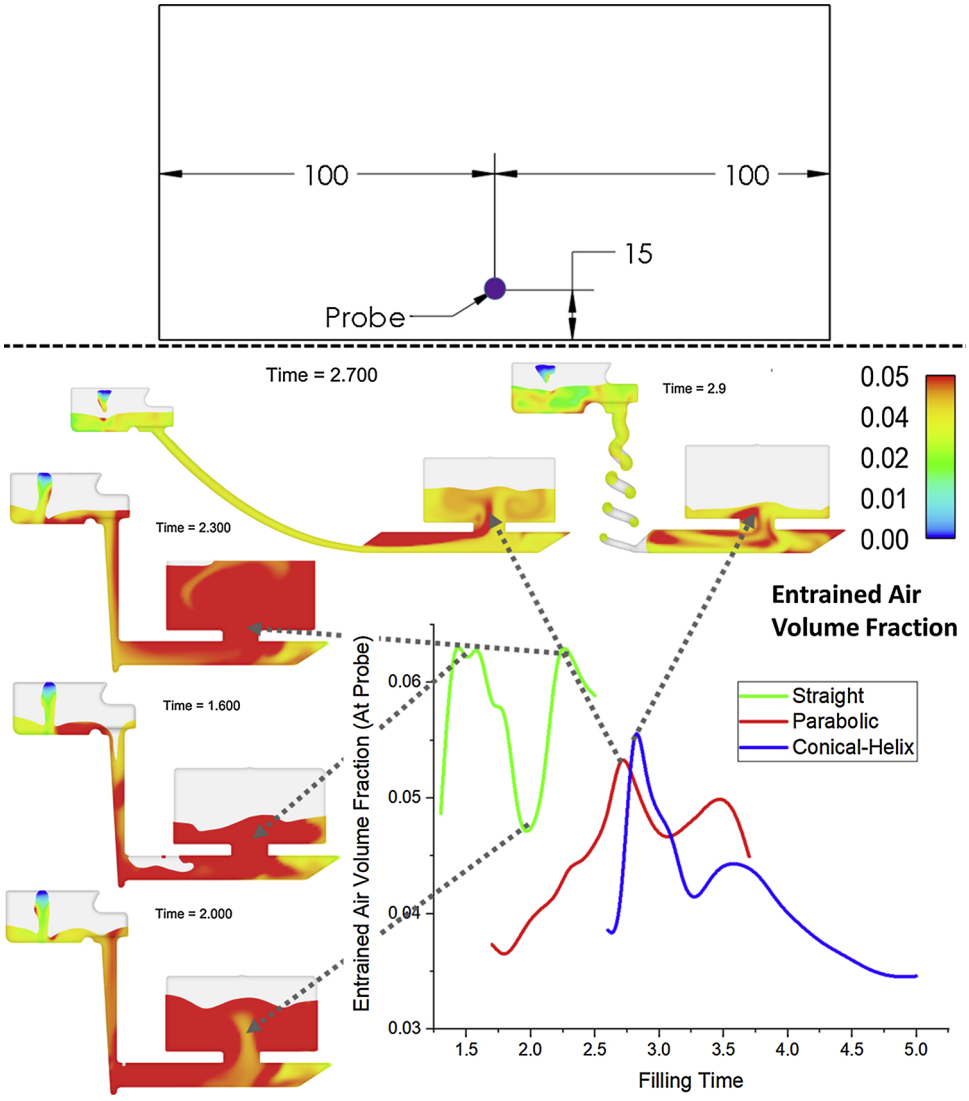

Fig. 14. Comparison of the fraction of entrained air volume measured by a probe at an identical location for all three sprued castings.

in this study are considered prevalent in reoxidation and formation of non-metallic inclusions in steel [74,75]. The pre-pour chemistry measured through optical emission spectroscopy (OES) is also similar to the post-pour chemistry of the parent-alloy measured using EDS as is shown in Table 3. Inconsistency in carbon composition in Table 3 is attributed to contamination during pouring. In 17-4 stainless steel alloy, inclusions that are found in this study are shown to affect the mechanical strength by initiating cracks on fracture surfaces [76].

6.2. Improvements in casting performance

Based on the 112 μm voxel resolution for CT scans used in this study, the scale of casting defects observed in this study is macroscopic. The defects observed in CT scans could be due to air entrapment, solidification shrinkage, dissolved gases, pouring defined dross and slag, and blowholes from unvented cores or reactions at the mold wall [72]. The surface of the casting was relatively homogeneous whereas the frequency and size of the voids was much greater towards the center plane of the casting. Fig. 20 compares the distribution of void space across the plate thickness for all three sprue designs and interestingly the profile follows a Gaussian distribution with the Gaussian mean at the mid-plane of the casting. Results from this study validate the center-line shrinkage phenomenon which is a result of directional solidification in castings where solidification is initiated from the mold walls and progress towards the center. It can be observed that SSC exhibits maximum center-line defect area of 1.5% whereas PSC has an area of only around 0.6% and it is negligble in CHSC.

The decrease in the total inclusions area in the microstructure of CHSC when compared to SSC could be either (1) due to decrease in total number of inclusions or (2) decrease in average size of individual inclusions. A one-way ANOVA statistical analysis was conducted to find of effect of each of these factors between each of the three groups viz. SSC, PSC and CHSC. The summary of the statistical analysis is presented in Table 4. It can be observed that no statistical significant difference was observed between the populations for inclusions count. However, a p-value far less than 0.05 was recorded for the effect of average inclusion area between SSC and CHSC; and a p-value of 0.042 was observed between SSC and PSC. This result shows that redesigning the sprue to render complex profiles such as parabolic and conical-helix significantly reduces the average size of inclusions when compared to SSC. Size of inclusion was found to increase with increase in turbulence and reoxidation [73]. Therefore, this study concludes that incorporation of mathematically optimized sprue profiles reduces turbulence which also reduces molten metal temperature to reduce shrinkage and hence, reoxidation in castings.

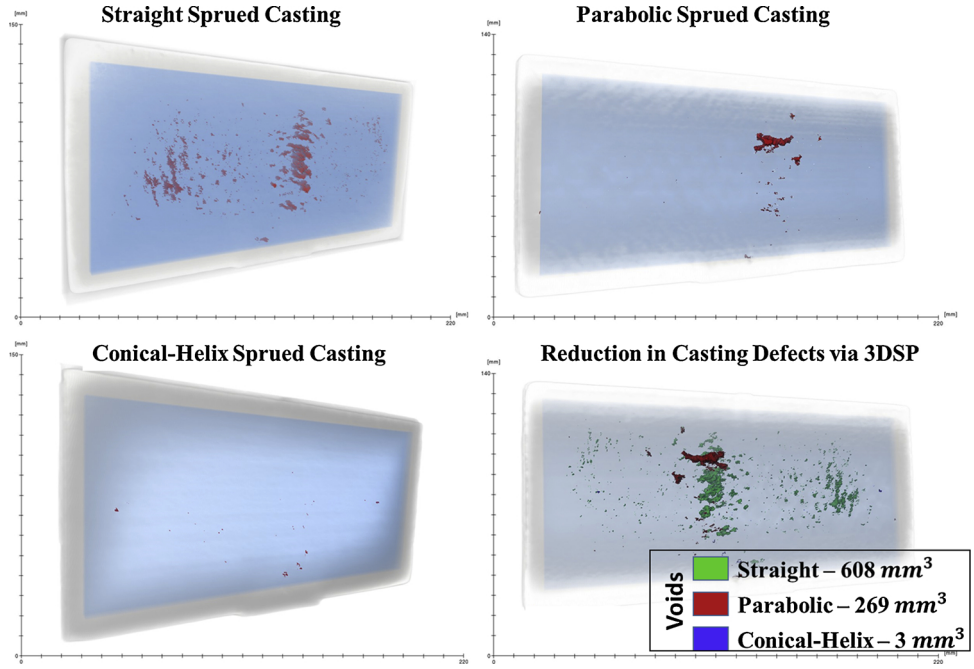

Fig. 15. CT Scan of (a) SSC (b) PSC (c) CHSC (d) Comparison of void space for all three sprue designs.

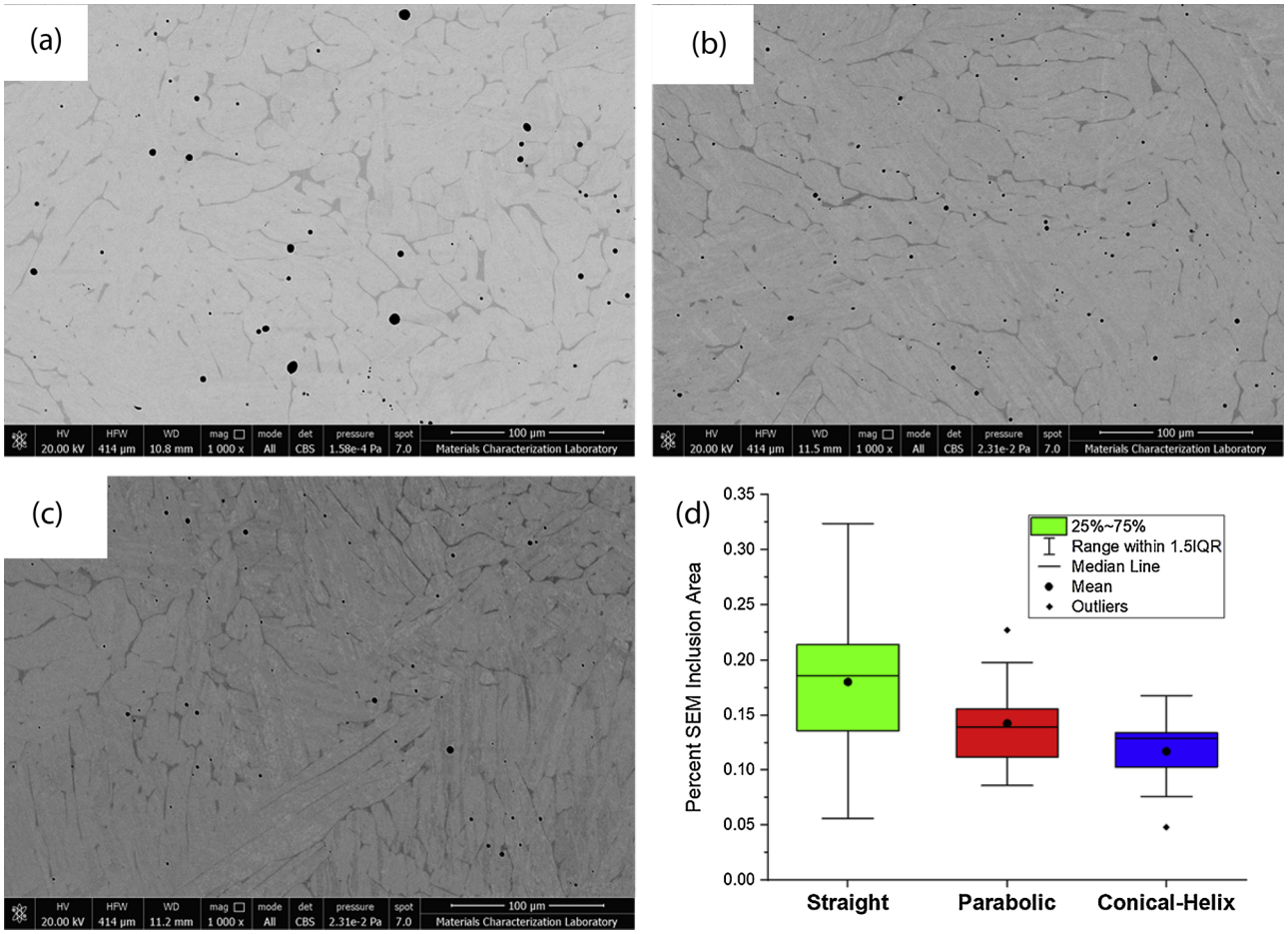

Fig. 16. SEM micrograph shown inclusions in specimens from (a) SSC (b) PSC (c) CHSC; (d) comparison of percent area inclusions on the microstructure.

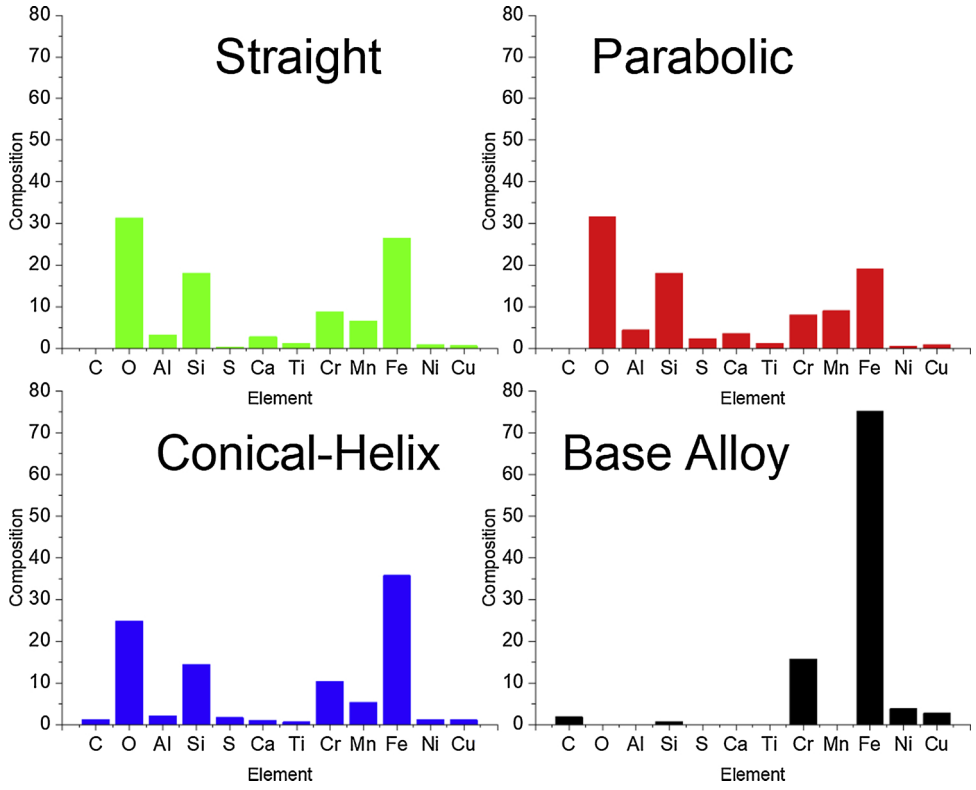

Fig. 17. Comparison of elemental composition of inclusions.

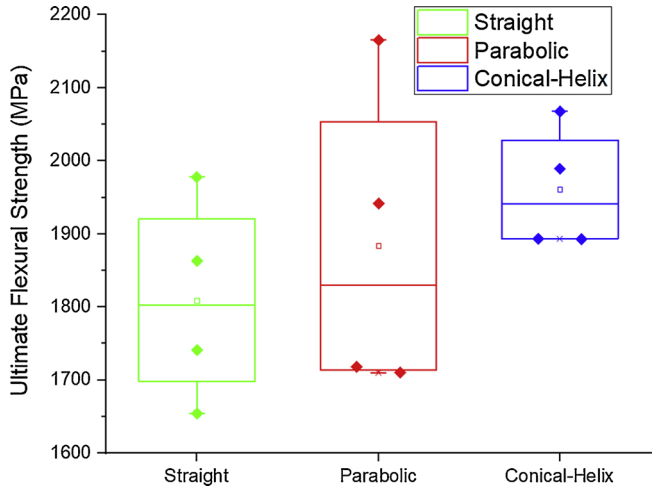

Fig. 18. Comparison of ultimate flexural strength of castings for all three sprue designs.

6.3. Effect of filters on non-conventional sprues

In order to isolate indigenous inclusions, another set of experiments were performed with 3″ × 3″ × 1″ fully sintered reticulated ceramic filters made of partially stabilized zirconia [77]. A filter is inserted for each of the three sprue designs at the top of the sprue in an effort to eliminate undesirable suspended phases from the melt prior to entering the subsequent gating system [78]. The results presented in Fig. 21 do not show evidence of significant differences in inclusion distribution or flexural strength between filtered and unfiltered castings for this specific filter placement and sprue design configurations. Ceramic filters could increase the number of inclusions downstream by shredding and raveling the oxide films to produce more defects [20]. In order to investigate the effects of gating system design on grain structure, samples from SSC and CHSC filtered castings were polished and etched with Vilella's reagent (1 g picric acid, 100 mL ethanol and 5 mL HCL) as per ASTM E407 standard [79]. No significant difference in grain structure was observed. It is widely known that grain size is defined by solidification rate which is not impacted by sprue design.

6.4. Novelty and viability of the optimization algorithm

As discussed earlier, maximum sprue length exists beyond which the metal would freeze in the gating system and not fill the casting because of thermal energy loss. Authors investigated this limit by designing an experiment similar to the fluidity tests [80] but the spiral cavity is designed for sprues instead of castings as shown in Fig. 22. Two molds featuring horizontal and vertical parting lines (categories 1 and 2 in Fig. 8) are fabricated through 3DSP and poured with 17-4 stainless steel alloy. The resulted castings are shown in Fig. 22 and it can be observed that the liquid metal froze after traversing 1200 mm in the sprue in both cases which establishes the repeatability of fluidity in the developed optimization algorithm.

By reducing melt flow turbulence, the conical-helix sprue also decreased mold wall (sand) erosion. Fig. 23 compares the as-cast surfaces between SSC and CHSC and it can be observed that the turbulence in SSC eroded the mold wall leading to intensive sand erosion. In contrast, the laminar flow in CHSC facilitated smooth filling and therefore no sand erosion is observed in the cast part.

In order to establish the manufacturability of a conical-helix sprue, the authors are currently experimenting with alloys that have different levels of sensitivity to turbulence, i.e. aluminum, 17-4 stainless steel and cast iron. Aluminum is known to have highest sensitivity towards turbulence when compared to cast iron and stainless steel. Fig. 24 shows the feasibility of CHSC for aluminum, 17-4 stainless steel and gray cast iron.

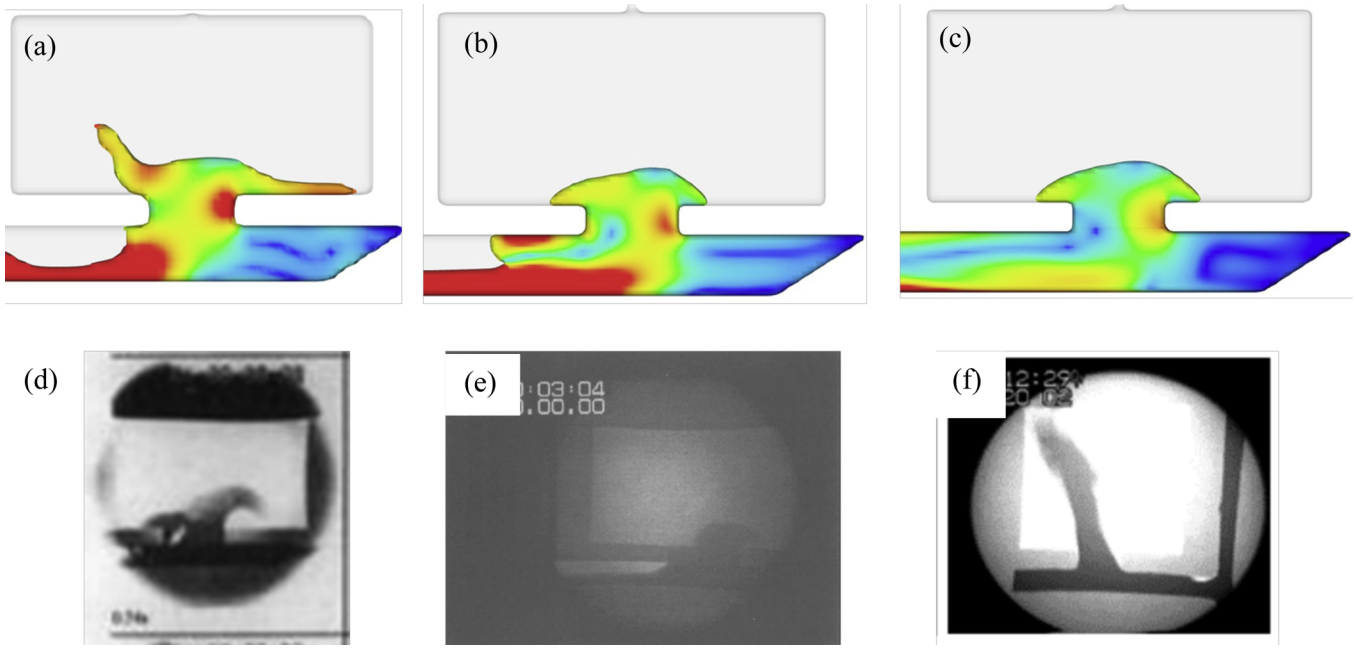

Fig. 19. Fountaining pattern comparison between CFD simulation of (a) SSC (b) PSC (c) CHSC; vs real-time X-ray radiograph of (d) aluminum (adopted from [65]) (e) Aluminum (adopted from [33]) (f) Gray Cast Iron (adopted from [45]).

Table 3
Chemical composition wt% of 17-4 stainless steel alloy measured using (a) OES before pouring (b) EDS after solidification.

17-4 Stainless Steel		C	Mn	Si	Cr	Ni	Mo	Cu	Fe
Pre-pour (a)	OES	0.03	0.55	0.80	16.2	3.77	0.1	2.72	75.4
Post-Pour (b)	EDS	2.09	0.53	0.67	15.7	3.91	0.0	2.74	74.4

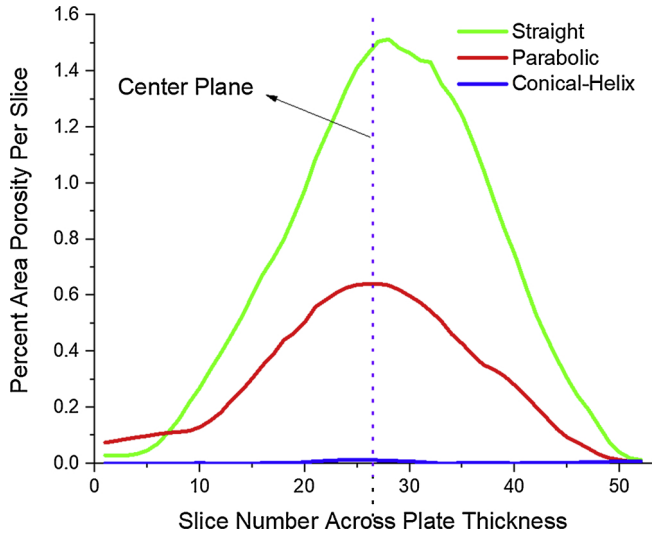

Fig. 20. Casting defects across plate thickness follows Gaussian distribution for castings from three sprue designs.

Table 4
One-way ANOVA p-value between population means, *shows statistical significance.

ANOVA Group		*p*-value from one-way ANOVA	
		Average Size	Inclusion Count
Straight (SSC)	Parabolic (PSC)	0.043*	0.77
Straight (SSC)	Conical-Helix (CHSC)	0.007*	0.22
Parabolic (PSC)	Conical-Helix (CHSC)	0.85	0.103

7. Conclusions

This research is the first known study that utilizes the design freedom offered by 3D Sand-Printing process to redesign sprue which is well established as the element of gating system which causes agitation in melt flow. Numerical model and optimization algorithm for novel sprue profiles (parabolic and conical-helix) are developed to mitigate casting defects caused by surface turbulence. These validated numerical models advance traditional casting hydrodynamic principles by minimizing thermal energy loss during mold filling while constraining melt flow velocities in gating system. Molds featuring the two optimized sprue profiles (parabolic and conical-helix) and also a straight sprue for comparison are 3D sand-printed and poured with 17-4 PH. Multiple analysis of sprue designs for 17-4 stainless steel alloy including computational flow simulations, computed tomography scanning, SEM, EDS and three-point flexural testing are conducted to investigate casting performance and the main conclusions are:

1 CFD simulations shows that both optimized parabolic (PSC) and conical-helix sprue (CHSC) designs reduce surface turbulence of the metal below critical velocity during mold filling.
2 CT scan results shows that casting defect volume can be reduced by 99.5% using conical-helix sprue (CHSC) design. The results also validate centerline shrinkage phenomenon in casting based on Gaussian distribution of casting defects across the thickness of the plate.
3 Conical-helix sprued casting (CHSC) exhibits significantly reduced inclusion and significantly higher ultimate flexural strength when compared to straight sprued casting. Globular inclusions that

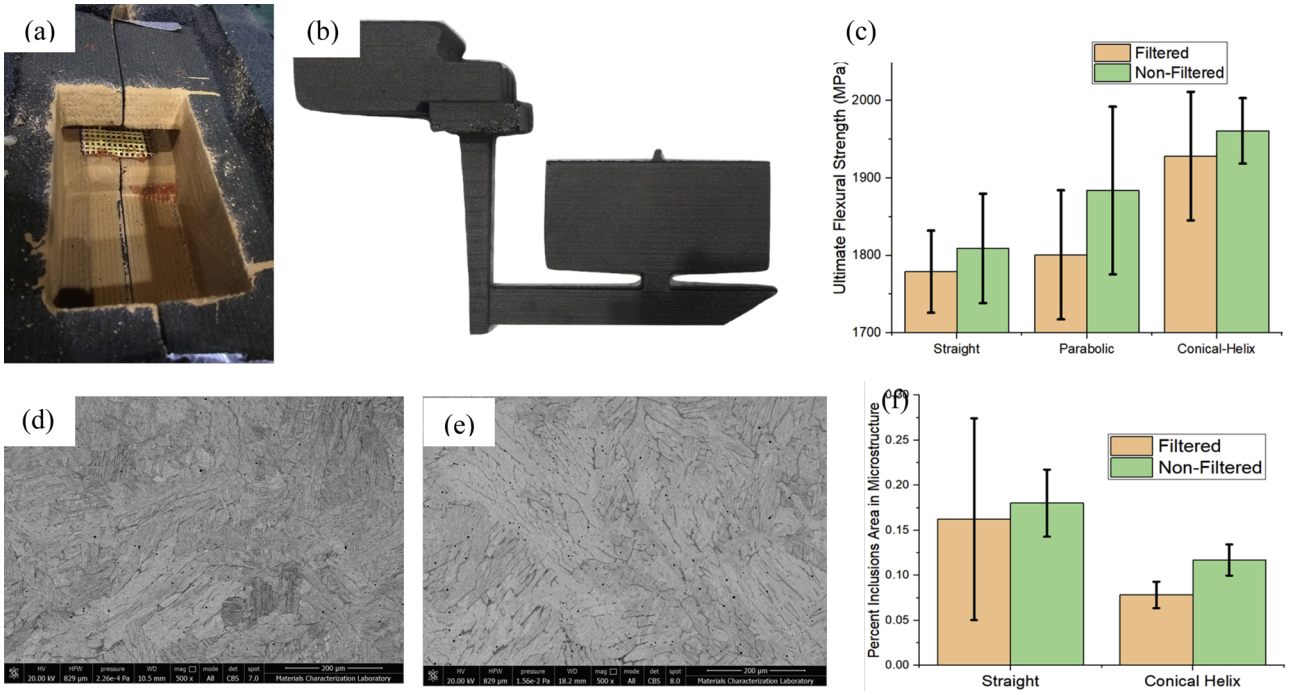

Fig. 21. (a) Filter inserted at the top of the sprue in the mold (b) Filtered SSC (c) No significant effect of filtering on ultimate flexural strength (d) Microstructure of etched filtered SSC (e) Microstructure of etched filtered CHSC (f) No significant effect of filtering on oxide inclusion area.

Fig. 22. Fluidity spiral test using sprue optimization and 3DSP mold.

primarily consist of alumina, silica and manganese oxides are observed and did not vary based on sprue design.

4 The manufacturability of conical-helix sprue (CHSC) is established using multiple design approaches and among them is the novel platform of Hybrid Molding.

Future work will include measuring bend loss factor for incorporation into head loss formulation. Other characterization techniques including impact test, tensile test, compressive test, fractography, fatigue test, EBSD, surface roughness will be performed to critically investigate the variation in casting performance due to redesign of gating systems. Ongoing efforts include efforts on real-time process monitoring by embedding miniature Internet of Things (*IoT*) sensors into the 3DSP molds.

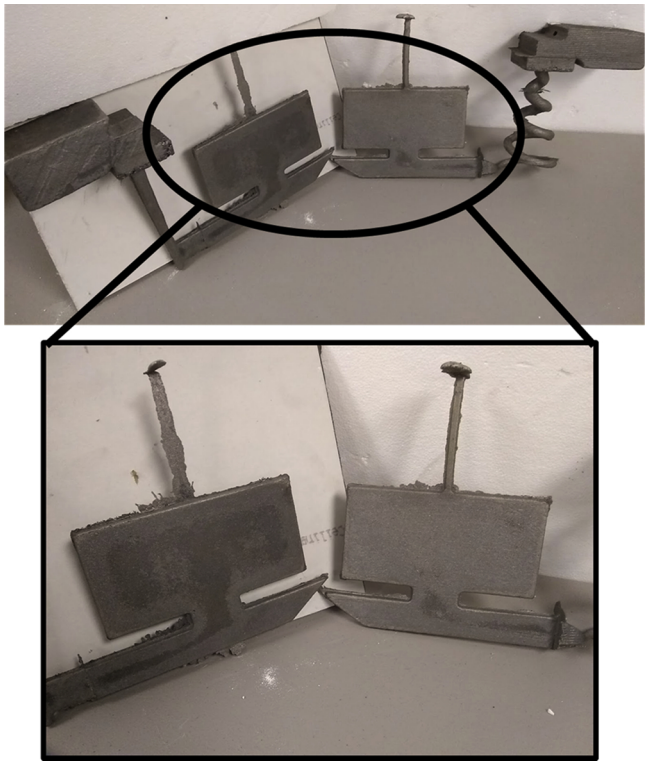

Fig. 23. Comparison of as-cast surfaces of SSC and CHSC demonstrates that quiescently filled CHSC features no sand erosion.

Author contributions

Research design, manufacturing, sample preparation, data processing, interpretation and drafting the manuscript by SRS. Manufacturing of molds, pouring, supplies and critical review of the manuscript by TB.

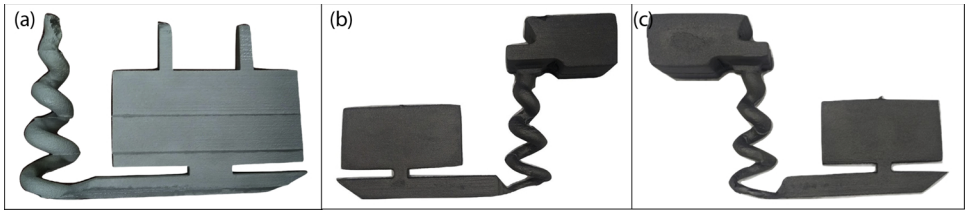

Fig. 24. Demonstrating manufacturability of optimized conical-helix sprues for (a) Aluminum 319 alloy (b) 17-4 stainless steel alloy (c) Class 30 Gy Cast Iron.

Material characterization, data processing, and critical review of the manuscript by PL. Research design, manufacturing, and critical review of the manuscript by GM.

Acknowledgements

The authors would like to thank America Makes for providing financial support through AM4MC grant, Hazleton Casting Company for providing experimental resources, Penn State MCL SEED grant for material characterization and Flow 3D-CAST for providing extended research license. The assistance of Dr. Robert Voigt and Dr. Eric MacDonald in the development of this work is greatly appreciated. The authors would like to thank Xi Gong, Maryam Tilton, Swapnil Sinha, Baily Thomas, Jiayi Wang and Gregory Bicknell for their technical support and help in specimen preparation and testing.

Appendix A. Supplementary data

Supplementary material related to this article can be found, in the online version, at doi:https://doi.org/10.1016/j.addma.2018.12.009.

References

[1] Markets and markets, January. Metal Casting Market.: Global Forecast Until 2025, Accessible on: (2018) https://www.marketsandmarkets.com/Market-Reports/metal-casting-market-23885716.html.
[2] Pennsylvania Foundry Association, March. OSHA'S Proposed Silica Rule Threatens Foundry Industry. Plymouth Meeting, PA, Accessible on: (2016) http://www.pfaweb.org/news/2016/3/11/oshas-proposed-silica-rule-threatens-foundry-industry-1.
[3] J. Dańko, R. Dańko, M. Holtzer, Reclamation of used sands in foundry production, Metalurgija 42 (3) (2003) 173–177.
[4] E.S. Almaghariz, B.P. Conner, L. Lenner, R. Gullapalli, G.P. Manogharan, B. Lamoncha, M. Fang, Quantifying the role of part design complexity in using 3D sand printing for molds and cores, Int. J. Metalcast. 10 (3) (2016) 240–252.
[5] J. Wang, S.R. Sama, G. Manogharan, Re-thinking design methodology for castings: 3D sand-printing and topology optimization, Int. J. Metalcast. (2018) 1–16.
[6] Chee Kai Chua, Kah Fai Leong, Zhong Hong Liu, Rapid tooling in manufacturing, Handbook of Manufacturing Engineering and Technology (2013) 1–22.
[7] P. Jain, A.M. Kuthe, Feasibility study of manufacturing using rapid prototyping: FDM approach, Procedia Eng. 63 (2013) 4–11.
[8] J. Campbell, Complete Casting Handbook: Metal Casting Processes, Metallurgy, Techniques and Design, 2nd edition, Butterworth-Heinemann, 2015.
[9] R. Gopalan, N.K. Prabhu, Oxide bifilms in aluminium alloy castings–a review, Mater. Sci. Technol. 27 (12) (2011) 1757–1769.
[10] J. Campbell, The consolidation of metals: the origin of bifilms, J. Mater. Sci. 51 (1) (2016) 96–106.
[11] R. Raiszadeh, W.D. Griffiths, A method to study the history of a double oxide film defect in liquid aluminum alloys, Metal. Mater. Trans. B 37 (6) (2006) 865–871.
[12] X. Cao, J. Campbell, The nucleation of Fe-rich phases on oxide films in Al-11.5 Si-0.4 Mg cast alloys, Metal. Mater. Trans. A 34 (7) (2003) 1409–1420.
[13] A. Modaresi, A. Safikhani, A.M.S. Noohi, N. Hamidnezhad, S.M. Maki, Gating system design and simulation of gray iron casting to eliminate oxide layers caused by turbulence, Int. J. Metalcast. 11 (2) (2017) 328–339.
[14] F.N. Bakhtiarani, R. Raiszadeh, Healing of double-oxide film defects in commercial purity aluminum melt, Metal. Mater. Trans. B 42 (2) (2011) 331–340.
[15] F.H. Basuny, M. Ghazy, A.R.Y. Kandeil, M.A. El-Sayed, Effect of casting conditions on the fracture strength of Al-5 Mg alloy castings, Adv. Mater. Sci. Eng. 2016 (2016).
[16] J. Campbell, Castings, 2nd edition, Butterworth-Heinemann, 2003.
[17] X. Dai, X. Yang, J. Campbell, J. Wood, Influence of oxide film defects generated in filling on mechanical strength of aluminium alloy castings, Mater. Sci. Technol. 20 (4) (2004) 505–513.
[18] M. Divandari, J. Campbell, Mechanisms of Bubble Damage in Castings. University of Birmingham. PhD Dissertation, The School of Metallurgy and Materials, 2001.
[19] J. Mi, R.A. Harding, J. Campbell, Effects of the entrained surface film on the reliability of castings, Metal. Mater. Trans. A 35 (9) (2004) 2893–2902.
[20] B. Sirrell, J. Campbell, Mechanism of filtration in reduction of casting defects due to surface turbulence during mold filling (97-11), Trans. Am. Foundrymen's Soc. 105 (1997) 645–654.
[21] X.Y. Zhao, Z.L. Ning, F.Y. Cao, S.G. Liu, Y.J. Huang, J.S. Liu, J.F. Sun, Effect of double oxide film defects on mechanical properties of As-cast C95800 alloy, Acta Metallurgica Sinica (Eng. Lett.) 30 (6) (2017) 541–549.
[22] C. Nyahumwa, N.R. Green, J. Campbell, Effect of mold-filling turbulence on fatigue properties of cast aluminum alloys (98-58), Trans. Am. Foundrymen's Soc. 106 (1998) 215–224.
[23] N.R. Green, J. Campbell, Influence of oxide film filling defects on the strength of Al-7Si-Mg alloy castings (94-114), Trans. Am. Foundrymen's Soc. 102 (1994) 341–348.
[24] S.H. Majidi, J. Griffin, C. Beckermann, Simulation of air entrainment during mold filling: comparison with water modeling experiments, Metal. Mater. Trans. B 49 (5) (2018) 2599–2610.
[25] X. Cao, J. Campbell, Oxide inclusion defects in Al-Si-Mg cast alloys, Can. Metall. Q. 44 (4) (2005) 435–448.
[26] K. Bangyikhan, Effects of Oxide Film, Fe-Rich Phase, Porosity and Their Interactions on Tensile Properties of Cast Al-Si-Mg Alloys. PhD Thesis, University of Birmingham. School of Metallurgy and Materials, 2005.
[27] R. Raiszadeh, W.D. Griffiths, A semi-empirical mathematical model to estimate the duration of the atmosphere within a double oxide film defect in pure aluminum alloy, Metal. Mater. Trans. B 39 (2) (2008) 298–303.
[28] G.E. Bozchaloei, N. Varahram, P. Davami, S.K. Kim, Effect of oxide bifilms on the mechanical properties of cast Al–7Si–0.3 Mg alloy and the roll of runner height after filter on their formation, Mater. Sci. Eng.: A 548 (2012) 99–105.
[29] J. Campbell, Invisible macrodefects in castings, Le J. de Physique IV 3 (C7) (1993) C7–861.
[30] S.M.A. Boutorabi, J. Campbell, J.J. Runyoro, Critical gate velocity for film-forming casting alloys; a basis for process specifications, Trans. Am. Foundrymen's Soc. 100 (1992) 225–234.
[31] J. Brown, Foseco non-Ferrous Foundryman's Handbook, 1st edition, Butterworth-Heinemann, 1999.
[32] T.R. Rao, Metal Casting: principles and Practice. New Age International, 1st edition, (1996).
[33] X. Yang, T. Din, J. Campbell, Liquid metal flow in moulds with off-set sprue, Int. J. Cast Met. Res. 11 (1) (1998) 1–12.
[34] A.K. Bińi, Gas entrainment by plunging liquid jets, Chem. Eng. Sci. 48 (21) (1993) 3585–3630.
[35] C. Beckermann, Water modeling of steel flow, air entrainment and filtration, September, SFSA T&O Conference (1992).
[36] R.W. Ruddle, The running and gating of Sand casting, Inst. Met. Monogr. Rep. Ser. (1956) 19.
[37] R.E. Swift, J.H. Jackson, L.W. Eastwood, A study of principles of gating, AFS Trans. 57 (1949) 76–88.
[38] K.H. Renukananda, B. Ravi, Multi-gate systems in casting process: comparative study of liquid metal and water flow, Mater. Manuf. Processes 31 (8) (2016) 1091–1101.
[39] R. Cuesta, J.A. Maroto, D. Morinigo, I. De Castro, D. Mozo, Water analogue experiments as an accurate simulation method of the filling of aluminum castings, Trans.-Am. Foundrymens Soc. 114 (2006) 137–150.
[40] S.L. Nimbulkar, R.S. Dalu, Design optimization of gating and feeding system through simulation technique for sand casting of wear plate, Perspect. Sci. 8 (2016) 39–42.
[41] H. Iqbal, A.K. Sheikh, A. Al-Yousef, M. Younas, Mold design optimization for sand casting of complex geometries using advance simulation tools, Mater. Manuf. Processes 27 (7) (2012) 775–785.
[42] Z. Sun, H. Hu, X. Chen, Numerical optimization of gating system parameters for a magnesium alloy casting with multiple performance characteristics, J. Mater. Process. Technol. 199 (1-3) (2008) 256–264.
[43] E. Rabinovich, Mécanique Des Fluides, Comptes Rendus (Doklady) de L'Académie Des Sciences de L'URSS Vol. 54 Édition de l'Académie des sciences de l'URSS, 1946 No. 5, p. 391.
[44] M.B.N. Shaikh, S. Ahmad, A. Khan, M. Ali, August. Optimization of multi-gate systems in casting process: experimental and simulation studies, IOP Conference Series: MaTerials Science and Engineering IOP Publishing 404 (2018) No 1. 012040.
[45] W. Sun, C.E. Bates, Visualizing defect formation in gray iron castings using real time X-rays, Trans. Am. Foundry Soc. Vol. 111 (2003) 859–867.
[46] F.R. Juretzko, D.M. Stefanescu, Comparison of mold filling simulation with high speed video recording of real-time mold filling, AFS Trans. 113 (2005) 1–11.
[47] D. Kothe, D. Juric, K. Lam, B. Lally, Numerical recipes for mold filling simulation (April), Proceedings of the Eighth International Conference on Modeling of Casting, Welding, and Advanced Solidification Processes (1998).
[48] P. Cleary, J. Ha, V. Alguine, T. Nguyen, Flow modelling in casting processes, Appl.

Math. Modell. 26 (2) (2002) 171–190.
[49] J. Jezierski, R. Dojka, K. Janerka, Optimizing the gating system for steel castings, Metals 8 (4) (2018) 266.
[50] C.E. Esparza, M.P. Guerrero-Mata, R.Z. Ríos-Mercado, Optimal design of gating systems by gradient search methods, Comput. Mater. Sci 36 (4) (2006) 457–467.
[51] J. Kor, X. Chen, H. Hu, Multi-objective optimal gating and riser design for metal-casting, July, Control Applications, (CCA) Intelligent Control, IEEE, 2009, pp. 428–433.
[52] S.R. Sama, J. Wang, G. Manogharan, Non-conventional mold design for metal casting using 3D sand-printing, J. Manuf. Processes. (2018).
[53] F.Y. Hsu, M.R. Jolly, J. Campbell, A multiple-gate runner system for gravity casting, J. Mater. Process. Technol. 209 (17) (2009) 5736–5750.
[54] R. Ahmad, N. Talib, Experimental study of vortex flow induced by a vortex well in sand casting, Revue de Métallurgie–Int. J. Metal. 108 (3) (2011) 129–139.
[55] H. Shangguan, J. Kang, C. Deng, Y. Hu, T. Huang, 3D-printed shell-truss sand mold for aluminum castings, J. Mater. Process. Technol. 250 (2017) 247–253.
[56] M. Tiryakioglu, D.R. Askeland, C.W. Ramsay, Fluidity of 319 and A356: an experimental design approach, Trans.-Am. Foundrymens Soc. (1995) 17–26.
[57] W.S. Hwang, R.A. Stoehr, Fluid flow modeling for computer-aided design of castings, JOM 35 (10) (1983) 22–29.
[58] S.E. Haaland, Simple and explicit formulas for the friction factor in turbulent pipe flow, J. Fluids Eng. 105 (1) (1983) 89–90.
[59] D. Vaghasia, Gating System Design Optimization for Sand Casting. Indian Institute of Technology Bombay. M. Tech Dissertation. Manufacturing Engineering, (2009).
[60] American Society of Mechanical Engineers. Standards Committee B46. Classification, & Designation of Surface Qualities. (2003). Surface texture: Surface roughness, waviness and lay. Amer Society of Mechanical.
[61] N. Wukovich, G. Metevelis,). Gating: the Foundryman's dilemma or fifty years of data and still asking how? 93Rd AFS Casting Congress, (1989).
[62] P. Muenprasertdee, Solidification Modeling of Iron Castings Using SOLIDCast. West Virginia University. MS Thesis, Industrial and Management Systems Engineering, 2007.
[63] D. Snelling, H. Blount, C. Forman, K. Ramsburg, A. Wentzel, C. Williams, A. Druschitz, The effects of 3D printed molds on metal castings, In Proceedings of the Solid Freeform Fabrication Symposium, (2013), pp. 827–845.
[64] American Society of Mechanical Engineers. Standards Committee E28. Mechanical Testing. (2004). Standard Test Methods for Bend Testing of Material for Ductility E290-14. Amer Society for Mechanical.
[65] B. Sirrell, M. Holliday, J. Campbell, Benchmark testing the flow and solidification modeling of AI castings, Jom 48 (3) (1996) 20–23.
[66] M. Masoumi, H. Hu, J. Hedjazi, M. Boutorabi, Effect of gating design on mold filling, Trans. Am. Foundry Soc. 113 (113) (2005) 185–196.
[67] P.C. Belding, The Control of non-Metallic Inclusions in Cast Steel. Organ State University. MS Thesis, Metallurgical Engineering, 1971.
[68] W.S. Rasband, Image J. US, National Institutes of Health, Bethesda, MD, USA, 1997.
[69] J.A. Griffin, C.E. Bates, Ladle Treating, Pouring, and Gating for the Production of Clean Steel Castings, Technical Steering Committee, Steel Founders' Society of America, 1991.
[70] L. Wang, C. Beckermann, Prediction of reoxidation inclusion composition in casting of steel, Metal. Mater. Trans. B 37 (4) (2006) 571–588.
[71] X. Dai, X. Yang, J. Campbell, J. Wood, Effects of runner system design on the mechanical strength of Al–7Si–Mg alloy castings, Mater. Sci. Eng.: A 354 (1-2) (2003) 315–325.
[72] R. Monroe, Porosity in castings, AFS Trans. 113 (2005) 519–546.
[73] R.B. Tuttle, M. Masoumi, H. Hu, J. Hedjazi, M. Boutorabi, Macroinclusion sources within the steel casting process, American Foundry Society Proceedings, (2010).
[74] M. Harris, V. Richards, R.J. O'Malley, S.N. Lekakh, Chicago, ILEvolution of Non-Metallic Inclusions in Foundry Steel Casting Processes. Proceedings of the 69th Annual Technical and Operating Conference, Steel Founders' Society of America2015, December, Evolution of Non-Metallic Inclusions in Foundry Steel Casting Processes. Proceedings of the 69th Annual Technical and Operating Conference, Steel Founders' Society of America (2015).
[75] K.D. Carlson, C. Beckermann, Modeling of reoxidation inclusion formation during filling of steel castings, Proceedings of the 58th Annual Technical and Operating Conference, Steel Founders' Society of America. Chicago, IL. Paper 4.6, (2004).
[76] A.S. Murthy, S.N. Lekakh, D.C. Van Aken, Role of niobium and effect of heat treatments on strength and toughness of modified 17-4 PH stainless steel, Proceedings of the 63rd Annual Technical and Operating Conference, Steel Founders' Society of America. Chicago, IL. Paper 3.4, (2010).
[77] ASK Chemicals, Udicell And Exactflo Filters, Accessible on: Available: http://www.ask-chemicals.com/fileadmin/user_upload/Download_page/foundry_products_brochures/EN/Udicell_Exactflo_Overview_EN.pdf.
[78] P.F. Wieser, Filtration of Irons and Steels. Foundry Processes – Their Chemistry and Physics, Springer, Boston, MA, 1988, pp. 495–512.
[79] American Society of Mechanical Engineers. Standards Committee E04. Metallography. (2015). Standard practice for microetching metals and alloys E407-07. Amer Society for Mechanical.
[80] M. Di Sabatino, Fluidity of Aluminium Foundry Alloys. Norwegian University of Science and Technology. PhD Thesis, Materials Science and Engineering, 2005.